Multi-satellite data depicts record-breaking methane leak from a well blowout

Luis Guanter[1,2*], Javier Roger[1], Shubham Sharma[3], Adriana Valverde[1], Itziar Irakulis-Loitxate[4,1], Javier Gorroño[1], Xin Zhang[3], Berend J. Schuit[3], Joannes D. Maasakkers[3], Ilse Aben[3], Alexis Groshenry[5], Antoine Benoit[5], Quentin Peyle[5], Daniel Zavala-Araiza[2]

[1]*Research Institute of Water and Environmental Engineering (IIAMA), Universitat Politècnica de València, Spain.*
[2]*Environmental Defense Fund, Amsterdam, Netherlands*
[3]*SRON Netherlands Institute for Space Research, Leiden, Netherlands*
[4]*International Methane Emissions Observatory, United Nations Environment Programme, Paris, France*
[5]*Kayrros, Paris, France*

*To whom correspondence should be addressed; E-mail: lguanter@fis.upv.es

Accidental blowouts in oil and gas wells can result in large and prolonged methane emissions, which are often unreported when happening in remote places. We use satellites to document a massive methane release from a well blowout in Kazakhstan's Karaturun East oil field in 2023. The 205-day methane leak resulted in a total emission of 127$\pm$37 kt of methane, surpassing the emissions from all previously reported accidents and highlighting the pivotal role of satellites in detecting and quantifying large methane leaks around the planet.

Human-induced methane emissions are responsible for about 30% of the global warming since the pre-industrial period[1]. The oil and gas production industry accounts for a large share of those emissions[2]. There is increasing evidence that emissions from the oil and gas production sector, and in particular from high-emitting point sources (also known as super-emitters[3]), are substantially underestimated in national inventories and industry reporting frameworks[4;5]. Conversely, the mitigation of oil and gas emissions has been found to be technically feasible and cost-effective[6].

Methane super-emitters in the oil and gas industry are usually linked to unexpected infrastructure failures, such as blowouts during drilling, completion, or production activities in oil and gas wells. Well blowouts result in uncontrolled releases of substantial amounts of natural gas, which consists primarily of methane. These accidents often occur in remote areas and are episodic, which complicates the acquisition of surface and airborne measurements for a proper documentation of the associated gas emissions. However, this was not the case of the 2015 Aliso Canyon blowout event, which happened at a Southern California Gas Company's storage facility in Los Angeles (USA). This blowout led to a massive methane leak between 23 October 2015 and 11 February 2016. An airborne campaign with 13 research-aircraft flights could be deployed to characterise the event. It was estimated that a total of 97.1 metric kilotons (kt) of methane were released into the atmosphere, with peak emission rates of 60 metric tons of gas per hour (t/h)[7], which make it the largest single natural gas leak in U.S. history.

A growing constellation of methane-sensitive satellites is now improving our ability to detect and monitor large methane leaks. The Sentinel-5P/TROPOMI mission and a number of high spatial resolution missions are the key assets in this constellation. TROPOMI was launched in 2018 and provides a systematic daily global surveillance of the largest methane emissions[8;9]. In contrast, the high-resolution missions have a sparse spatio-temporal sampling as compared with TROPOMI, but scan the Earth at a much higher spatial resolution, which enables the detection of smaller plumes and the possibility of attributing those to facility-level sources. Among these high-resolution missions we find the GHGSat private constellation[10;11], specifically designed for methane and carbon dioxide mapping at 25–50 m resolution, and the EnMAP, PRISMA and EMIT scientific missions, which also have a relatively high sensitivity to methane[12–14]. There are some examples of the potential of satellites in this constellation to document methane emissions from well blowouts: Thompson et al. conducted the first detection of an individual methane plume with observations of the Aliso Canyon event by the Hyperion high-resolution spectroscopy demonstration mission[15]; Pandey et al. used one TROPOMI overpass to estimate the emissions caused by a shale gas well blowout in Ohio (USA)[16]; Maasakkers et al. used six TROPOMI overpasses and gas flaring data from the VIIRS satellite instrument to estimate emissions from a natural gas well blowout in Louisiana (USA)[17]; Cusworth et al. combined observations from TROPOMI, GHGSat and PRISMA (four observations in total) to characterise the emissions from a 20-day leak event due to a gas well blowout in the Eagle Ford Shale (USA)[18]. All these well-documented blowouts happened in the USA, at sites relatively accessible to well operators and mitigation teams.

[Figure 1 about here.]

In this work, we have generated a dense time series of more than hundred satellite observations to document a massive methane emission event triggered by a well blowout at the Karaturun East oil field in Kazakhstan's Mangistau region. According to media reports, the well blowout and subsequent fire happened on the morning of 9 June 2023 during exploration works at well 303[19] (Fig. 1a). The fire destroyed different pieces of safety equipment, leading to a loss of well control and a 10-m high fire blaze. Days later, a 15-m wide crater was formed by the collapse of rocks around the wellhead, which prevented an early seal of the well. The first attempt to halt the flow of gas consisted of pumping thousands of tons of water through two injection holes between 13 October and 20 November. This action mitigated the gas leak, but did not completely resolve it. The flow of gas and the fire could finally be stopped on 25 December 2023 by injecting heavy drilling mud via a special-purpose probe, which connected with the wellbore of the accident well at a depth of about 1000 m[20].

Satellites are the only means to document the methane emissions following the blowout. The leak was first detected in TROPOMI daily global methane concentration data[19] (Fig. S1). The exact location and date of the blowout could be confirmed with data from the Sentinel-2 multispectral radiometer, which flew over the site hours after the accident. The evolution of the leak was then monitored with TROPOMI and a range of high-resolution missions (including PRISMA, EnMAP, EMIT, GHGSat and the Sentinel-2 and Landsat-8/9 multispectral radiometers), some of which were specifically tasked to acquire data over the site. Extremely large methane plumes were detected during the entire time series (Fig. 1b-e). The satellite data were processed with state-of-the-art algorithms for the detection and quantification of methane plumes from space, optimised for the particular plume intensities and site characteristics of this event (Methods).

We detect methane plumes from the site 115 times throughout the 9 June to 25 December 2023 time period. After quality screening of all the detected plumes, we retain 48 for the quantification of emission rates (Methods, Fig. 2). We obtain flux rates between 3.6 ± 1.3 and 63 ± 42 t/h, with typical values between 20 and 50 t/h (Fig. 2a, Supplementary Fig. S2, and Supplementary Table S1 and S2). The most substantial emission rates occur in the weeks following the blowout (Fig. 2a). Plume intensity gradually decreases over time until the leak repair on 25 December. Notably, a large plume (12 ± 3 t/h) was detected by GHGSat on 25 December, which suggests that the satellite flew over the site shortly before the final repair action on the same day. Three subsequent observations on 1, 12 and 14 January 2024 confirm the definitive cessation of the leak.

[Figure 2 about here.]

We utilize a time series of fire radiative power derived from the VIIRS FIRMS satellite product to track the fire intensity during the event (Methods). We also use observations from high resolution satellites to detect fire at the site, although those observations do not provide quantitative estimates of fire activity. We find that the strongest fire occurred immediately after the well blowout, with sustained high intensity for about 20 days (Fig. 2b). Subsequently, fire activity persisted throughout the event, as indicated by the active fire detections from the high resolution satellites. The fire intensity in this event (radiative power below 4 MW for the majority of days with recordings) is actually substantially lower than that of regular flares in oil and gas installations, and also than the intensity of the fires measured during the Louisiana 2019 event[17], where the radiative power was typically in the 10–50 MW range) and a clear inverse relationship between fire activity and methane emissions was found (Supplementary Fig. S3). The relatively low intensity of the fire at the Karaturun East site would indicate that only a small fraction of the gas outflow was flared. We hypothesize that the combustion efficiency during this event was low due to the 2-phase oil and gas mixture expected for this exploration well located on an oil field[21].

To give context to the magnitude of the methane plumes detected during the entire Karaturun East leak, the majority of plumes identified in this event exceed 10 t/h, which is comparable to the largest individual plumes detected using global TROPOMI data worldwide[8;9]. We obtain an estimate of 127±37 kt for the total amount of methane released to the atmosphere during the event (Methods), which is substantially larger than the total emission of 97 kt reported for the 2015 Aliso Canyon blowout (Fig. 2c). The total emission from the Karaturun event is also considerably greater than those estimated for the massive releases from the Ohio 2018[16] and the Louisiana 2019[17] blowout events (60±15 kt and 21–63 kt, respectively). Only the sabotage of the Nord Stream 1 and 2 subsea twin pipelines in the Baltic Sea on 26 September 2022, for which a total of 420-490 kt has been estimated[22], may have led to greater emissions than the Karaturun 2023 blowout event.

Our results show that the 2023 well blowout in Kazakhstan's Karaturun East oil field has likely caused the largest methane emission from an infrastructure accident ever documented. The detection and quantification of this leak has only been possible because of the recent availability of methane-sensitive satellites. It is unknown how many of such large methane leaks from oil and gas infrastructure failures may have occurred in the last decades around the world, and how this may have led to underestimated emission inventories. The new era of methane monitoring from space, boosted by international initiatives such as the Methane Alert and Response System (MARS)[23] implemented by the United Nations Environment Programme, will be crucial for the detection and quantification of large methane leaks around the world.

Methods

Satellite data

We generated a dense time series of methane observations over the Karaturun East site using TROPOMI and high-resolution satellite missions. The latter included observations from the GHGSat private satellite constellation, which offers the highest sensitivity to methane for this type of high-emitting point source, and from the EnMAP (German Aerospace Agency, Germany), PRISMA (Italian Space Agency, Italy) and EMIT (NASA Jet Propulsion Laboratory, USA), which are public scientific missions with a relatively similar configuration, a medium-high sensitivity to methane, and an open data policy. Acquisitions from the less sensitive Sentinel-2 and Landsat multispectral radiometers were also used for plume detection, and in 5 dates with optimal observation conditions, for quantification. A total of 115 plumes were detected throughout the 9 June to 25 December 2023 time period (26 from TROPOMI and 89 from the high resolution satellites). After quality control, 48 of those plumes (15 from TROPOMI and 33 from the high resolution satellites) were retained for the quantification of emissions.

Satellites were also used to monitor fire activity at the site. Fire radiative power data from the Fire Information for Resource Management System (FIRMS) based on VIIRS data were used to assess the evolution of fire intensity. In addition, the observations from the high resolution satellites used for methane mapping were also utilised to detect smaller active fires at the site, although these could not be quantified.

Quantification of methane plumes with high spatial resolution satellites

Consolidated processing algorithms were used to infer emission rates from the high spatial resolution missions.

For the retrieval of methane plume information from EnMAP, PRISMA and EMIT data, which are the bulk of our high-resolution dataset, we adapted the widely-used matched-filter approach to deal with the large plumes and high methane concentration values found during the Karaturun East leak. This included the implementation of a log-normal version of the matched filter and the removal of plume pixels when calculating the statistics needed for the matched-filter, as described in Pei et al.[24]. The ΔXCH_4 maps obtained with this retrieval were screened for quality (cloud-free, no retrieval artifacts, no substantial fractions of the plume lying outside the image area). The selected high-quality observations were used for the subsequent flux rate estimation. We manually delineated the plumes and calculated the integrated methane enhancement (IME) which is the total mass of methane contained in the plume. The IME values were converted into flux rate estimates using the IME-based model[25], which relates the IME, the plume length, and an effective wind speed parameter (U_{eff}) to the flux rate. For U_{eff}, we used linear $U_{\text{eff}} - U_{10}$ models specifically derived for the typical ΔXCH_4 retrieval precision and plume length estimated for this event (simulated plumes are 5-10 km long). One common $U_{\text{eff}} - U_{10}$ model was used for EnMAP and PRISMA, which share the same 30-m resolution and retrieval precision, and a second one was derived for EMIT in order to account for EMIT's 60 m pixels (Supplementary Fig. S4). Uncertainties in flux rate estimates were derived assuming a 50% uncertainty in the input wind speed data, which is consistent with previous studies.

This radiance-to-flux rate processing chain (ΔXCH_4 retrieval, plume segmentation, IME-based Q estimation) has been validated with controlled methane release tests[26]. Still, since those controlled-release tests were made for much weaker plumes than the ones detected in this event, we used end-to-end simulations to test our ability to quantify flux rate for large plumes and the particular conditions of the Karaturun East site. This end-to-end simulation approach has already been used with hyperspectral and multispectral data[12;27]. The results show that our processing is able to produce reliable flux estimates for an 5–50 t/h emission range, which is comparable to the one found during the Karaturun East leak (Supplementary Fig. S5).

It must be remarked that we do not find any distortion of our ΔXCH_4 maps with the water vapour and smoke being potentially co-emitted by the source (Supplementary Fig. S6). We have verified this by generating water vapour anomaly maps using a similar retrieval method as the one we use for methane. The resulting water vapour maps show the expected turbulence patterns, but not water vapour plume superposed to the methane plumes. Also, we do not detect any smoke signal in the 2300 nm spectral window used for the methane retrievals, indicating that the smoke plumes have no relevant optical activity in this range, which has also been noted in previous studies[13].

Regarding the other classes of high resolution missions, the internal processing chain described in Jervis et al.[11] was applied for GHGSat data. GHGSat detection limits and flux rate estimation ability have been validated over the years using controlled-release tests[26]. Finally, in the case of the 5 points obtained from multispectral missions (Sentinel-2 and Landsat), we have followed the approach described in Gorroño et al.[27]. This consists of a two-step processing scheme, in which ΔXCH_4 maps are first derived with a multi-band and multi-pass retrieval, and the flux rates are subsequently estimated using the IME-based method.

Quantification of methane plumes with TROPOMI

TROPOMI (aboard Sentinel-5P)[28] observes methane with high precision at resolution of $5.5\times7\,\mathrm{km}^2$, allowing detection of the plume further downwind. We used the Weather Research and Forecast (WRF) version 4.1[29] to simulate the enhanced methane concentrations associated with the blowout at a resolution of $3\times3\,\mathrm{km}^2$ from June to December 2023. We then compared these modelled concentrations to TROPOMI data in a Bayesian inversion framework[30] to infer daily emissions rates. To obtain simulated plumes that best match TROPOMI, we ran WRF using two meteorological boundary conditions products and four planetary boundary layer physics schemes, and sampled the model at several timesteps around the TROPOMI overpass. Based on daily inversions with all model setups, we selected the simulations that gave the lowest posterior observation cost for each day to be used. We only report quantifications for days with clear plumes and good matches with simulated plumes based on visual inspection. To estimate uncertainty, we built an ensemble of inversions by varying critical inversion parameters such as data filtering and the selected simulation. We conservatively report the 2-standard deviation range from the ensemble as uncertainty. Details on the TROPOMI quantification approach are given in the Supplementary Text S1.

Quantification of total methane emission

We estimate a total of 127±37 kt of methane being released to the atmosphere between 9 June and 25 December. This amount was calculated through the integration of a polynomial fitted to the time series of Q estimates from the plume data passing the quality screening (Supplementary Figure S2). The estimation of the uncertainty associated to the total emission is the result of propagating the uncertainty from each Q estimate through the Q interpolation and curve integration using multivariate Monte Carlo simulations. We assume a 50% correlation between flux rate errors in order to account for both uncorrelated error components (e.g. plume shape changes) and correlated error components (e.g. same source area) (Supplementary Fig. S7).

List of Supplementary Materials

- Text S1
- Tables S1 and S2
- Figures S1–S7

References

1. Dhakal, S. *et al.* Emissions trends and drivers. In Shukla, P. *et al.* (eds.) *Climate Change 2022: Mitigation of Climate Change. Contribution of Working Group III to the Sixth Assessment Report of the Intergovernmental Panel on Climate Change*, book section 2 (Cambridge University Press, Cambridge, UK and New York, NY, USA).

2. Saunois, M. *et al.* The global methane budget 2000–2017. *Earth System Science Data* **12**, 1561–1623 (2020).

3. Zavala-Araiza, D. *et al.* Reconciling divergent estimates of oil and gas methane emissions **112**, 15597–15602 (2015).

4. Alvarez, R. A. *et al.* Assessment of methane emissions from the u.s. oil and gas supply chain. *Science* **361**, 186–188 (2018).

5. Hmiel, B. *et al.* Preindustrial 14CH4 indicates greater anthropogenic fossil CH4 emissions. *Nature* **578**, 409–412 (2020).

6. Ocko, I. *et al.* Acting rapidly to deploy readily available methane mitigation measures by sector can immediately slow global warming. *Environmental Research Letters* **16** (2021).

7. Conley, S. *et al.* Methane emissions from the 2015 Aliso Canyon blowout in Los Angeles, CA. *Science* **351**, 1317–1320 (2016).

8. Lauvaux, T. *et al.* Global assessment of oil and gas methane ultra-emitters. *Science* **375**, 557–561 (2022).

9. Schuit, B. J. *et al.* Automated detection and monitoring of methane super-emitters using satellite data. *Atmospheric Chemistry and Physics* **23**, 9071–9098 (2023).

10. Varon, D. J. *et al.* Satellite Discovery of Anomalously Large Methane Point Sources From Oil/Gas Production. *Geophysical Research Letters* **46**, 13507–13516.

11. Jervis, D. *et al.* The GHGSat-D imaging spectrometer. *Atmospheric Measurement Techniques* **14**, 2127–2140 (2021).

12. Guanter, L. *et al.* Mapping methane point emissions with the PRISMA spaceborne imaging spectrometer. *Remote Sensing of Environment* **265**, 112671 (2021).

13. Roger, J. *et al.* High-resolution methane mapping with the EnMAP satellite imaging spectroscopy mission. *IEEE Transactions on Geoscience and Remote Sensing* 1–1 (2024).

14. Thorpe, A. K. *et al.* Attribution of individual methane and carbon dioxide emission sources using EMIT observations from space. *Science Advances* **9**, eadh2391 (2023).

15. Thompson, D. R. *et al.* Space-based remote imaging spectroscopy of the Aliso Canyon CH4 superemitter. *Geophysical Research Letters* **43**, 6571–6578 (2016).

16. Pandey, S. *et al.* Satellite observations reveal extreme methane leakage from a natural gas well blowout **116**, 26376–26381 (2019).

17. Maasakkers, J. D. *et al.* Reconstructing and quantifying methane emissions from the full duration of a 38-day natural gas well blowout using space-based observations. *Remote Sensing of Environment* **270**, 112755 (2022).

18. Cusworth, D. H. *et al.* Multisatellite imaging of a gas well blowout enables quantification of total methane emissions. *Geophysical Research Letters* **48**, e2020GL090864.

19. Clark, A. & Gizitdinov, N. Scientists Say They've Detected a Huge Methane Leak in Kazakhstan. *Bloomberg* (2023-08-04).

20. Afanasiev, V. Kazakh operator halts gas fire at well that has been burning since June. *Upstream* (2023-12-27).

21. Understanding wellhead ignition as a blowout response. *Fuel* **243**, 622–629 (2019).

22. S. Harris et al. Renewed understanding of atmospheric methane emissions from the 2022 Nord Stream pipeline sabotage (2023). Submitted.

23. UNEP-IMEO. Methane Alert and Response System (MARS). https://www.unep.org/explore-topics/energy/what-we-do/methane/imeo-action/methane-alert-and-response-system-mars (2023). [Online; accessed 1-February-2024].

24. Pei, Z. *et al.* Improving quantification of methane point source emissions from imaging spectroscopy. *Remote Sensing of Environment* **295**, 113652 (2023).

25. Varon, D. J. *et al.* Quantifying methane point sources from fine-scale satellite observations of atmospheric methane plumes. *Atmospheric Measurement Techniques* **11**, 5673–5686 (2018).

26. Sherwin, E. D. *et al.* Single-blind validation of space-based point-source detection and quantification of onshore methane emissions. *Scientific Reports* **13**, 3836 (2023).

27. Gorroño, J., Varon, D. J., Irakulis-Loitxate, I. & Guanter, L. Understanding the potential of Sentinel-2 for monitoring methane point emissions. *Atmospheric Measurement Techniques* **16**, 89–107 (2023).

28. Lorente, A., Borsdorff, T., Martinez-Velarte, M. C. & Landgraf, J. Accounting for surface reflectance spectral features in tropomi methane retrievals. *Atmospheric Measurement Techniques* **16**, 1597–1608 (2023).

29. Powers, J. *et al.* The weather research and forecasting (wrf) model: Overview, system efforts, and future directions. *Bulletin of the American Meteorological Society* **98** (2017).

30. Jacob, D. J. *et al.* Quantifying methane emissions from the global scale down to point sources using satellite observations of atmospheric methane. *Atmospheric Chemistry and Physics* **22**, 9617–9646 (2022).

Acknowledgments

This research was funded by the European Space Agency through the HiResCH4 project (contract N.4000134929) and the IMEO Science Studies programme (contract DTIE23-EN6386). We are thankful to Jason McKeever and the GHGSat team for the acquisition and processing of the GHGSat data used in this study. Patrizia Sacco and Ettore Lopinto (Italian Space Agency, ASI) are thanked for the PRISMA acquisitions, and Nicole Pinnel (German Aerospace Center, DLR) and Sabine Chabrillat (GFZ German Research Centre for Geosciences) for the EnMAP acquisitions. We are grateful to Daniel J. Varon for the

WRF-LES modelled plumes used in this study. Correspondence and request for materials should be addressed to L.G.

Competing interests: The authors declare no competing interests.

List of Figures

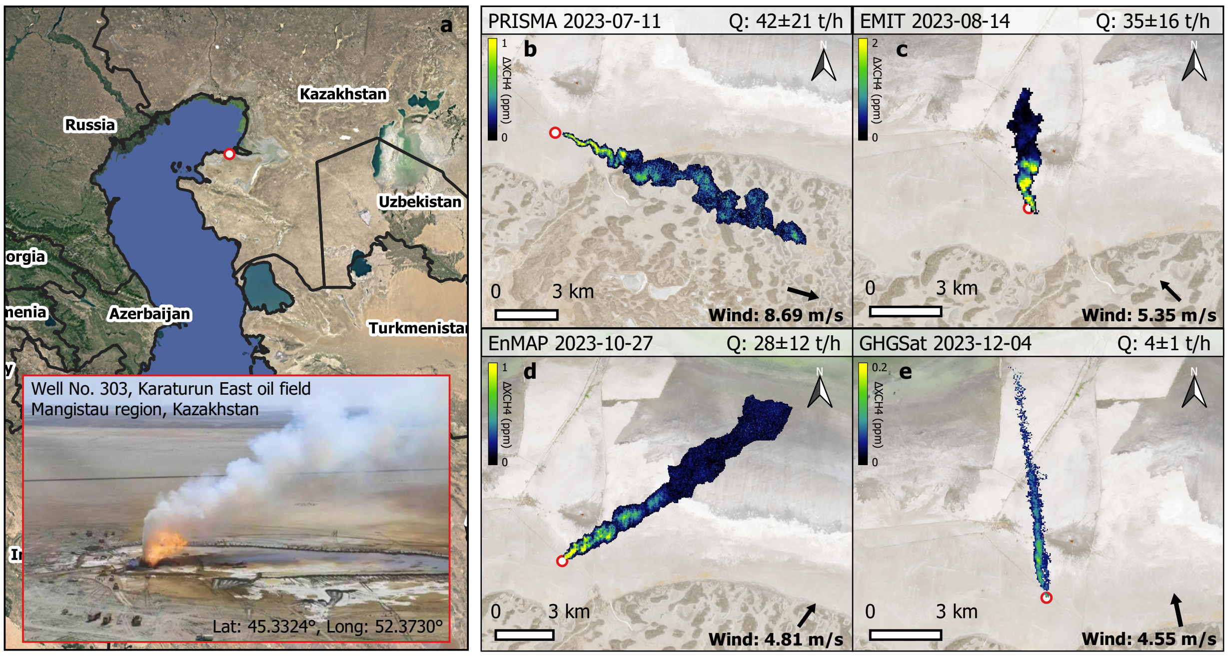

Figure 1: Site overview and examples of satellite-based methane plumes. **a**, Location of the Karaturun East oil field (45.3324°N, 52.3730°E) where the blowout happened on 9 June 2023, including a view of the active fire at the site (photo from Mangistau Regional Administration). **b-e**, Sample of methane plumes detected with the EnMAP, PRISMA, EMIT and GHGSat satellite sensors on different days. The color scale in the maps represent methane concentration enhancements above background methane levels (ΔXCH_4). The emission rate (Q) estimated for each plume is provided on the top right side of each map panel.

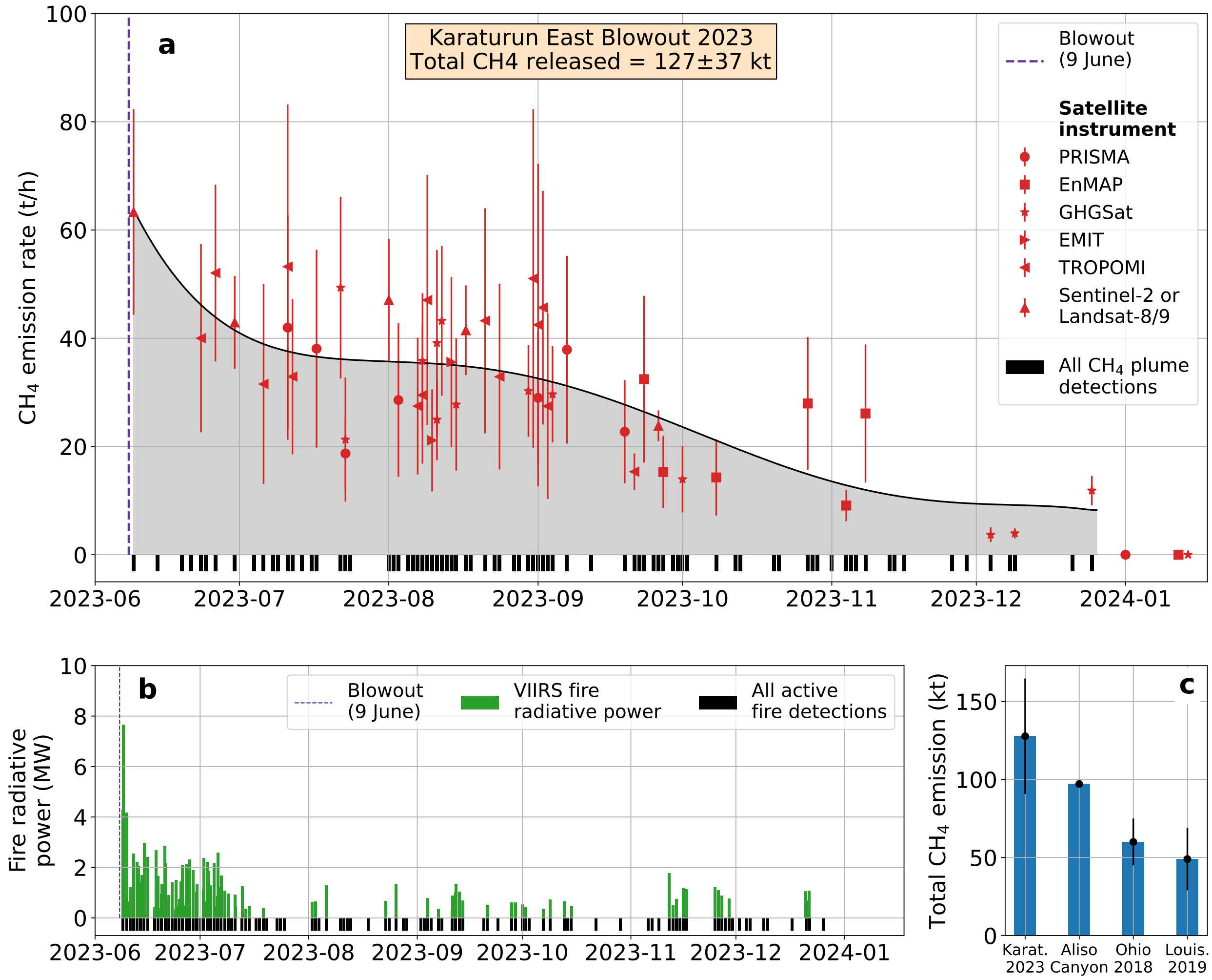

Figure 2: Quantification of methane emissions and fire intensity from the Karaturun East 2023 blowout. **a**, Time series of methane emission rates (in metric tonnes per hour, t/h) derived from the satellite observations which passed the quality screening (see also Supplementary Fig. S2). The black line and the shaded area represent the polynomial fit that has been integrated for the calculation of the total amount of methane released during the event. The black bars depict all satellite observations from which a plume could be detected, including those that could not be quantified. **b**, Time series of fire radiative power derived from the VIIRS FIRMS data product. The black bars depict all satellite detections of active fire at the site. **c**, Comparison of the total amount of methane released during the Karaturun East 2023 event with the Aliso Canyon 2015[7], Ohio 2018[16], and Lousiana 2019[17] blowout events also leading to massive methane emissions.

Supplementary Materials

Multi-satellite data depicts record-breaking methane leak from a well blowout

Luis Guanter[1,2*], Javier Roger[1], Shubham Sharma[3], Adriana Valverde[1], Itziar Irakulis-Loitxate[4,1], Javier Gorroño[1], Xin Zhang[3], Berend J. Schuit[3], Joannes D. Maasakkers[3], Ilse Aben[3], Alexis Groshenry[5], Antoine Benoit[5], Quentin Peyle[5], Daniel Zavala-Araiza[2]

[1]Research Institute of Water and Environmental Engineering (IIAMA), Universitat Politècnica de València, Spain.

[2]Environmental Defense Fund, Amsterdam, Netherlands

[3]SRON Netherlands Institute for Space Research, Leiden, Netherlands

[4]International Methane Emissions Observatory, United Nations Environment Programme, Paris, France

[5]Kayrros, Paris, France

*To whom correspondence should be addressed; E-mail: lguanter@fis.upv.es

List of Tables

List of Figures

Text S1. Quantification of methane plumes with TROPOMI

With daily global coverage, TROPOMI, onboard Sentinel-5P, enables global mapping of methane concentrations at 5.5×7 km^2 resolution using the shortwave infrared (SWIR) spectrum at 2.3 μm. For this analysis, we use version 02.05.00 of the TROPOMI-CH_4 operational product corrected for stripes[1] with a custom quality filter (qa value ≥ 0.4, SWIR aerosol optical thickness < 0.1, SWIR surface albedo > 0.05, surface classification $\neq 3$, and SWIR cloud fraction < 0.015).

Methane concentrations are simulated using the Weather Research and Forecast (WRF) version 4.1[2] around the blowout location at a 3×3 km^2 resolution for an area of 800×800 km^2 from June 2023 to December 2023. We perform simulations with both 6-hourly National Centre for Environmental Prediction (NCEP)[3] and hourly ERA5[4] meteorological fields. The 6-hourly Copernicus Atmosphere Monitoring Service (CAMS) atmospheric composition forecast data[5] is used to provide the initial and boundary conditions. We use anthropogenic emissions from EDGAR v7[6], except for fossil fuels, for which we use the updated Global Fuel Exploitation Inventory (GFEI)[7]. Wetland emissions come from WetCHARTs v1.3.[8]. To infer emissions, the Bayesian cost function J is minimized to optimize the state vector $\hat{\mathbf{x}}$[9]:

$$\hat{\mathbf{x}} = \mathbf{x}_A + \mathbf{S}_A \mathbf{K}^T (\mathbf{K}\mathbf{S}_A\mathbf{K}^T + \mathbf{S}_0^{-1}(\mathbf{y} - \mathbf{K}\mathbf{x}_A)) \tag{1}$$

where $\mathbf{x}_A$ is the prior state vector, considered 30 t/hr, $\mathbf{S}_A$ is the prior error covariance matrix assuming 10% uncertainty for the CAMS boundary conditions and 100% uncertainty for the blowout emissions, $\mathbf{K}$ is the Jacobian matrix, and $\mathbf{y}$ is the observational vector containing TROPOMI observations. The model output is resampled to match the TROPOMI pixel spatial footprint using TROPOMI averaging kernels. The observations and model are then aggregated to $0.2^\circ \times 0.2^\circ$ grids to negate model errors. $\mathbf{S}_0$, the observational error covariance matrix, is constructed as a diagonal matrix using the standard deviation of the difference between the prior modeled concentrations and TROPOMI observations.

To obtain a simulated plume that best matches the TROPOMI observed plume, we perform an ensemble of WRF simulations using: meteorological fields from either NCEP or ERA5, using four different planetary boundary layer physics options, and sampling the WRF outputs at the TROPOMI overpass time as well as up to 3 hours before and after the overpass time. Preliminary inversions are performed daily using the 56 simulated plumes, and the plumes with the lowest posterior observation cost function are selected. For the final inversion, we optimize the CAMS boundary conditions and the blowout emissions for each day. We only report quantifications for days with clear plumes, no potentially interfering downwind coastal artifacts, and good matches with simulated plumes based on visual inspection. We find that for all reported daily plume quantifications, the averaging kernel value for the blowout is above 0.5, showing the prior value has no significant impact on the estimated emissions. For estimating the uncertainty associated with the quantified emissions, an ensemble of inversions is computed by varying inputs and the assumptions used for the inversion[10]. This includes: increasing and decreasing the prior emissions for the blowout by a factor of 50%; using model outputs sampled every one hour before and after the overpass hour; using the second best plume match based on observation cost; performing the inversions using different aggregation resolutions $(0.15°, 0.25°)$; using TROPOMI data with highest quality flag of 1 (qa value $= 1$); using TROPOMI data without filtering for albedo, following the central limit theorem instead of using mean observational error, giving us a total of 1728 ensemble members for each day.

	Sensor	Acquisition date	Wind (m/s)	Q (t/h)	Q_err (t/h)
1	Sentinel-2	09/06/2023	3.0	63.3	42.0
2	Landsat 8-9	30/06/2023	2.9	42.9	14.6
3	PRISMA	11/07/2023	8.6	41.9	20.9
4	PRISMA	17/07/2023	7.3	38.0	18.2
5	GHGSAT	22/07/2023	4.6	49.3	16.8
6	GHGSAT	23/07/2023	1.5	21.2	11.4
7	PRISMA	23/07/2023	2.5	18.7	6.7
8	Landsat 8-9	01/08/2023	5.8	47.0	19.1
9	PRISMA	03/08/2023	8.9	28.5	14.1
10	GHGSAT	08/08/2023	4.5	35.8	12.5
11	EMIT	10/08/2023	5.6	21.1	9.4
12	GHGSAT	11/08/2023	2.8	39.1	17.2
13	GHGSAT	11/08/2023	5.6	24.9	7.5
14	GHGSAT	12/08/2023	5.1	43.2	13.8
15	EMIT	14/08/2023	5.3	35.6	15.7
16	GHGSAT	15/08/2023	2.8	27.7	12.2
17	Landsat 8-9	17/08/2023	3.9	41.4	15.4
18	GHGSAT	30/08/2023	6.3	30.2	8.5
19	PRISMA	01/09/2023	3.9	28.9	12.0
20	GHGSAT	04/09/2023	5.6	29.6	8.9
21	PRISMA	07/09/2023	5.7	37.8	17.3
22	PRISMA	19/09/2023	4.0	22.7	9.5
23	ENMAP	23/09/2023	6.9	32.4	15.4
24	Landsat 8-9	26/09/2023	4.9	23.8	9.3
25	ENMAP	27/09/2023	4.7	15.3	6.7
26	GHGSAT	01/10/2023	2.6	13.9	6.1
27	ENMAP	08/10/2023	8.5	14.2	7.0
28	ENMAP	27/10/2023	4.8	27.9	12.2
29	ENMAP	04/11/2023	1.9	9.0	2.9
30	ENMAP	08/11/2023	8.1	26.1	12.8
31	GHGSAT	04/12/2023	4.5	3.6	1.3
32	GHGSAT	09/12/2023	9.7	3.9	0.9
33	GHGSAT	25/12/2023	8.2	11.8	2.7

Table S1: Summary of the emission rates derived from the high-resolution satellite observations passing the quality screening process. This quality screening has removed the observations with cloud contamination, retrieval artifacts and plumes for which a substantial part of the tail lied outside the imaged area. Q refers to the flux rate estimated for each plume, and Q_err to the associated 1-σ uncertainty.

	Sensor	Acquisition date	Q (t/h)	Q_err (t/h)
1	TROPOMI	23/06/2023	40.0	17.3
2	TROPOMI	26/06/2023	52.0	16.3
3	TROPOMI	06/07/2023	31.5	18.4
4	TROPOMI	11/07/2023	53.2	29.9
5	TROPOMI	12/07/2023	32.9	14.3
6	TROPOMI	07/08/2023	27.4	12.6
7	TROPOMI	08/08/2023	29.5	12.6
8	TROPOMI	09/08/2023	47.0	23.1
9	TROPOMI	21/08/2023	43.2	20.8
10	TROPOMI	24/08/2023	32.9	17.1
11	TROPOMI	31/08/2023	51.0	31.3
12	TROPOMI	01/09/2023	42.4	29.7
13	TROPOMI	02/09/2023	45.6	21.5
14	TROPOMI	03/09/2023	27.4	17.1
15	TROPOMI	21/09/2023	15.3	3.3

Table S2: Summary of the emission rates derived from the TROPOMI satellite observations passing the quality screening process. This quality screening has consisted in the selection of only clear plumes and of good matches with simulated plumes based on visual inspection. Q refers to the flux rate estimated for each plume, and Q_err to the associated 1-σ uncertainty.

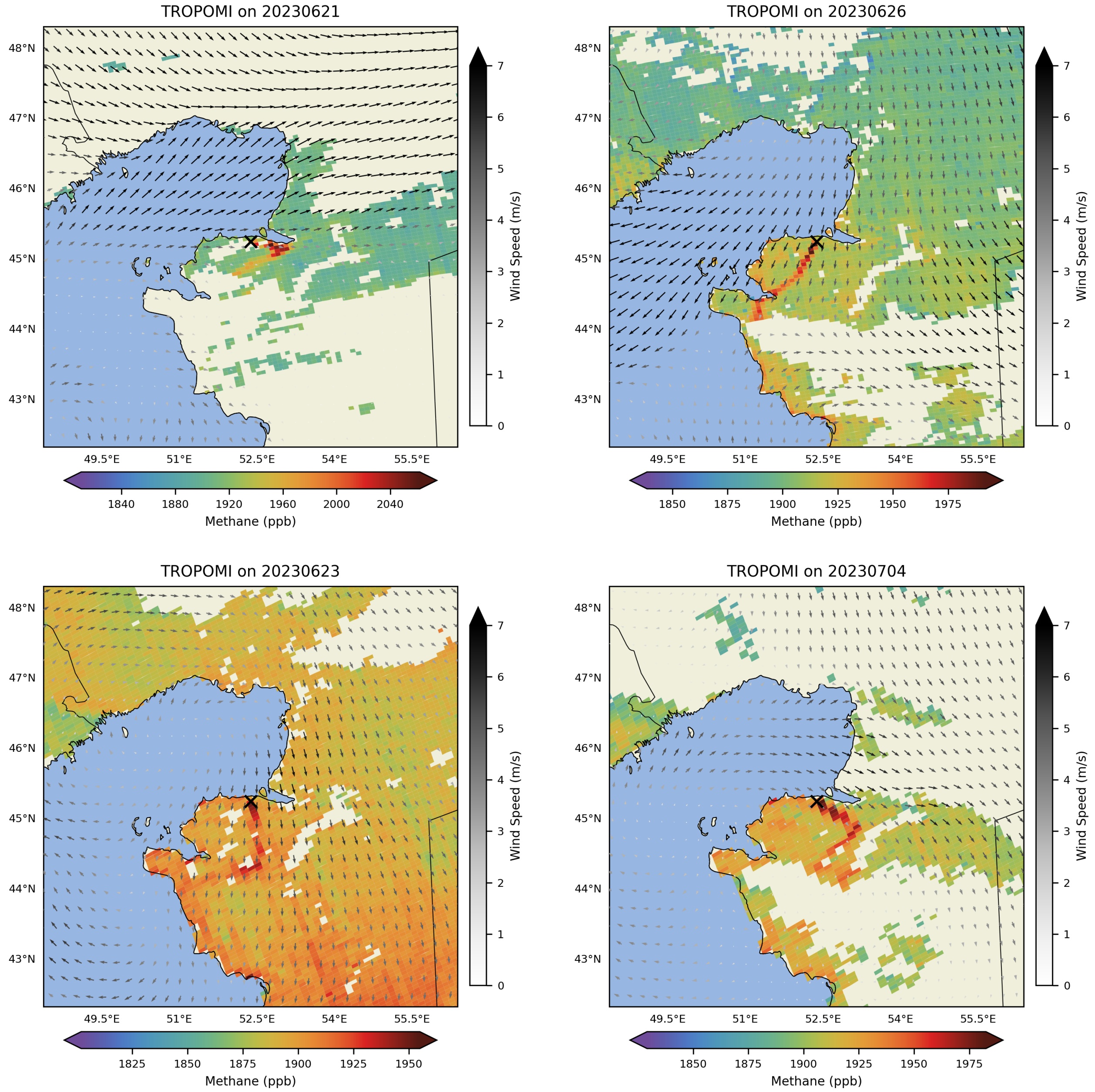

Figure S1: Methane column concentration maps for the first observations of the Karaturun 2023 leak by Sentinel-5P/TROPOMI. Data are from the TROPOMI-CH_4 operational product (02.05.00 version). The color scale indicates the total methane column concentration estimated from TROPOMI (as opposed to the concentration enhancement derived from the high resolution data). Arrows indicate wind intensity and direction.

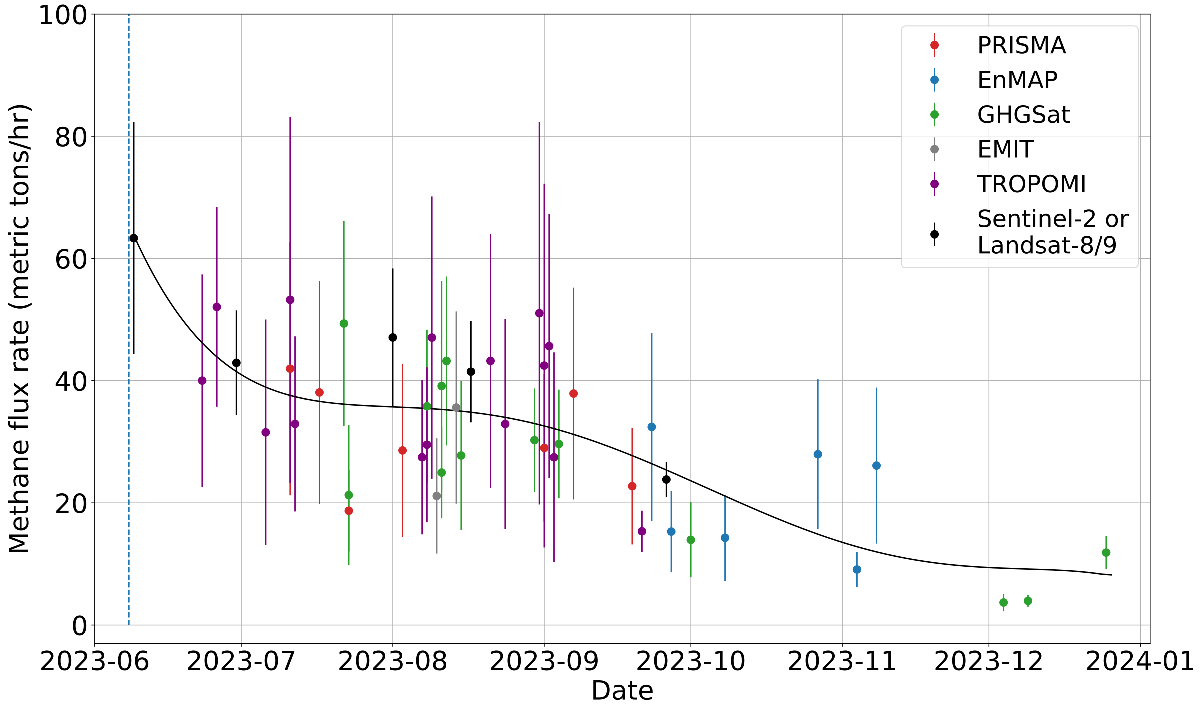

Figure S2: Time series of flux rate estimates obtained from the different satellites used in this work. The points represent the flux rate estimates for the 48 plumes retained for quantification after quality screening. This figure offers an alternative representation to that in Fig. 2 of the Main Text.

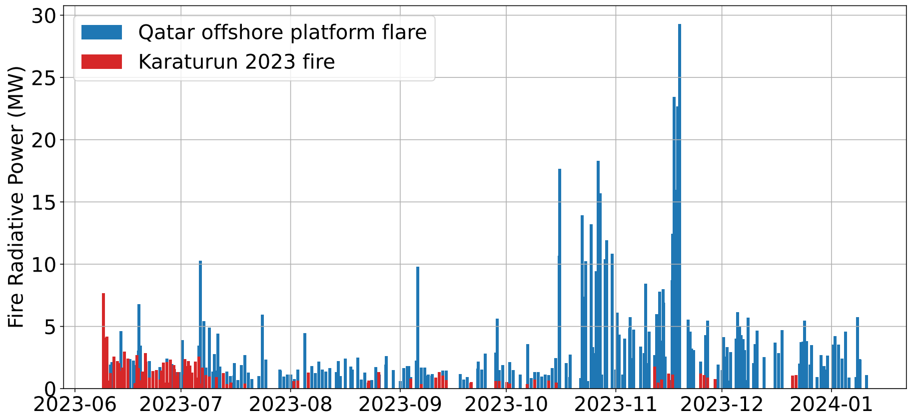

(a)

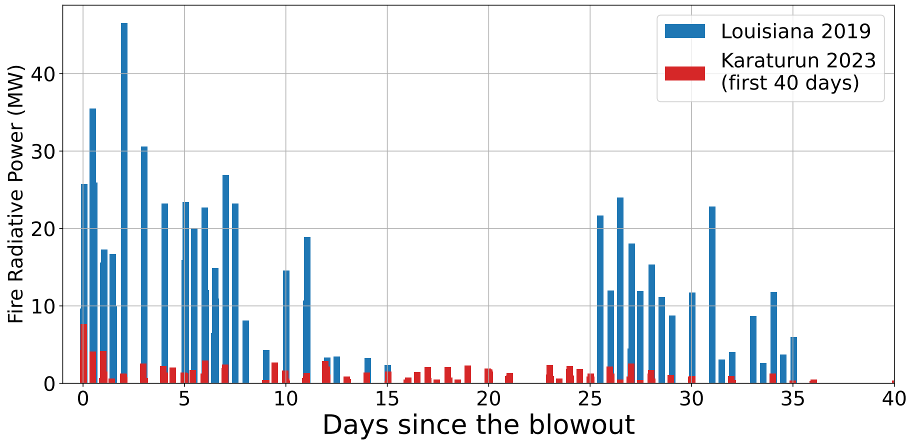

(b)

Figure S3: Comparison of the fire intensity at the Karaturun 2023 blowout site with that of other gas flaring events. (a) Regular flare in an offshore platform in Qatar (26.59°N, 52.00°E). (b) Fire intensity during the Louisiana 2019 event (Maasakkers et al., 2022), where gas burned first at the wellheads for two weeks, and then at a flare pit for 10 days, with a 10-day period in between during which the gas was vented. In both cases, fire intensity is proxied by the fire radiative power variable provided in the VIIRS Fire Information for Resource Management System (FIRMS) product.

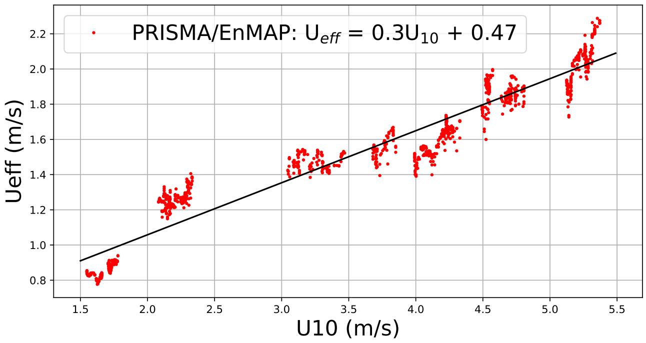

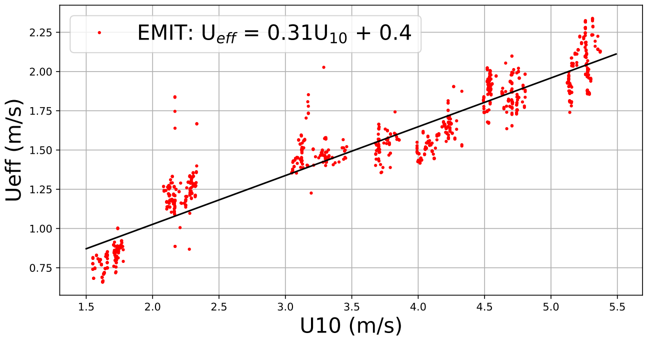

Figure S4: Empirical $U_{\mathrm{eff}} - U_{10}$ models for IME-based flux rate estimates from EnMAP, PRISMA and EMIT ΔXCH_4 retrievals. The linear models have been generated using a database of plumes simulated with a WRF-LES modeling approach. The plume simulations cover the flux rate range of 10–90 t/h, and are done for the ΔXCH_4 retrieval noise found in the Karaturun East site for those missions. Separate models have been generated for EnMAP-PRISMA and EMIT because of the different spatial sampling (30 m for EnMAP-PRISMA and 60 m for EMIT). Retrieval precision is assumed to be similar for EnMAP and PRISMA.

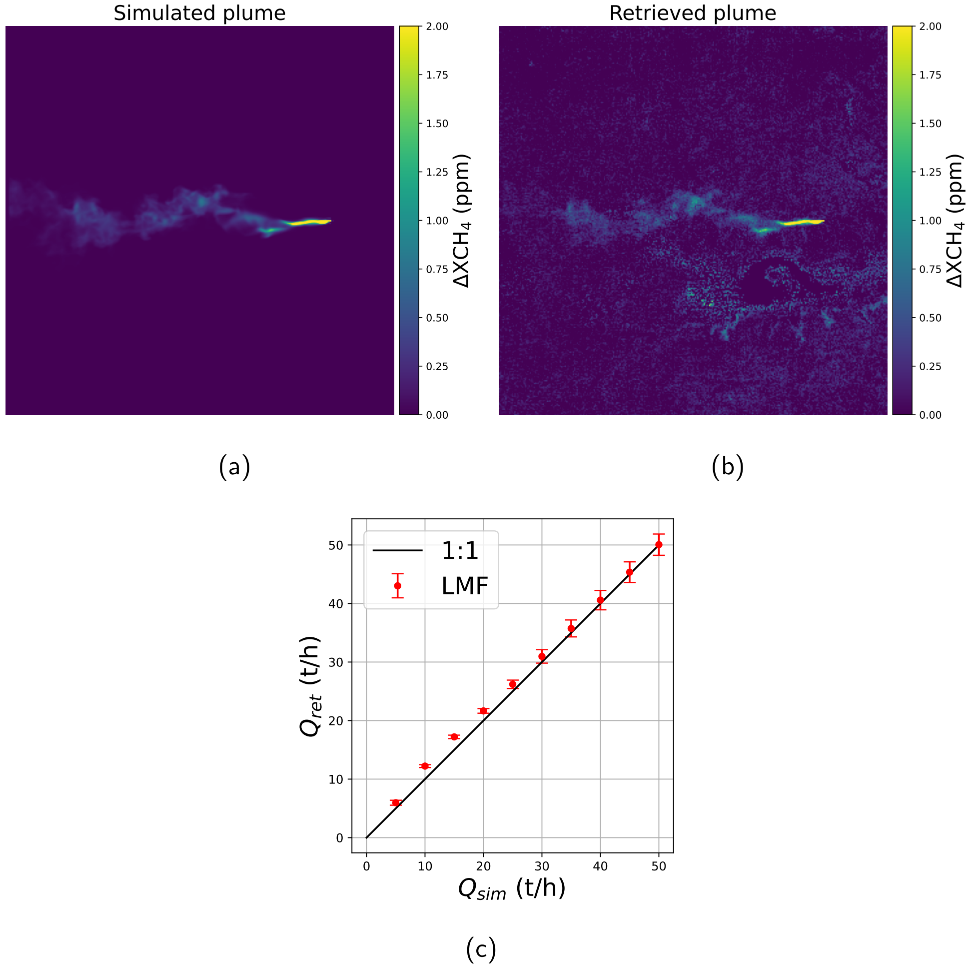

Figure S5: Verification of ΔXCH_4 retrievals and flux rate estimates from hyperspectral data with end-to-end simulations. (a), Simulated methane plume (25 t/h) added to a real PRISMA radiance dataset. (b), Methane plume retrieved from the processing of the resulting PRISMA radiance dataset using the ΔXCH_4 retrieval scheme implemented for this study. (c), Comparison of the input and estimated flux rates (Q_{sim} and Q_{ret}, respectively) from the entire end-to-end simulation process.

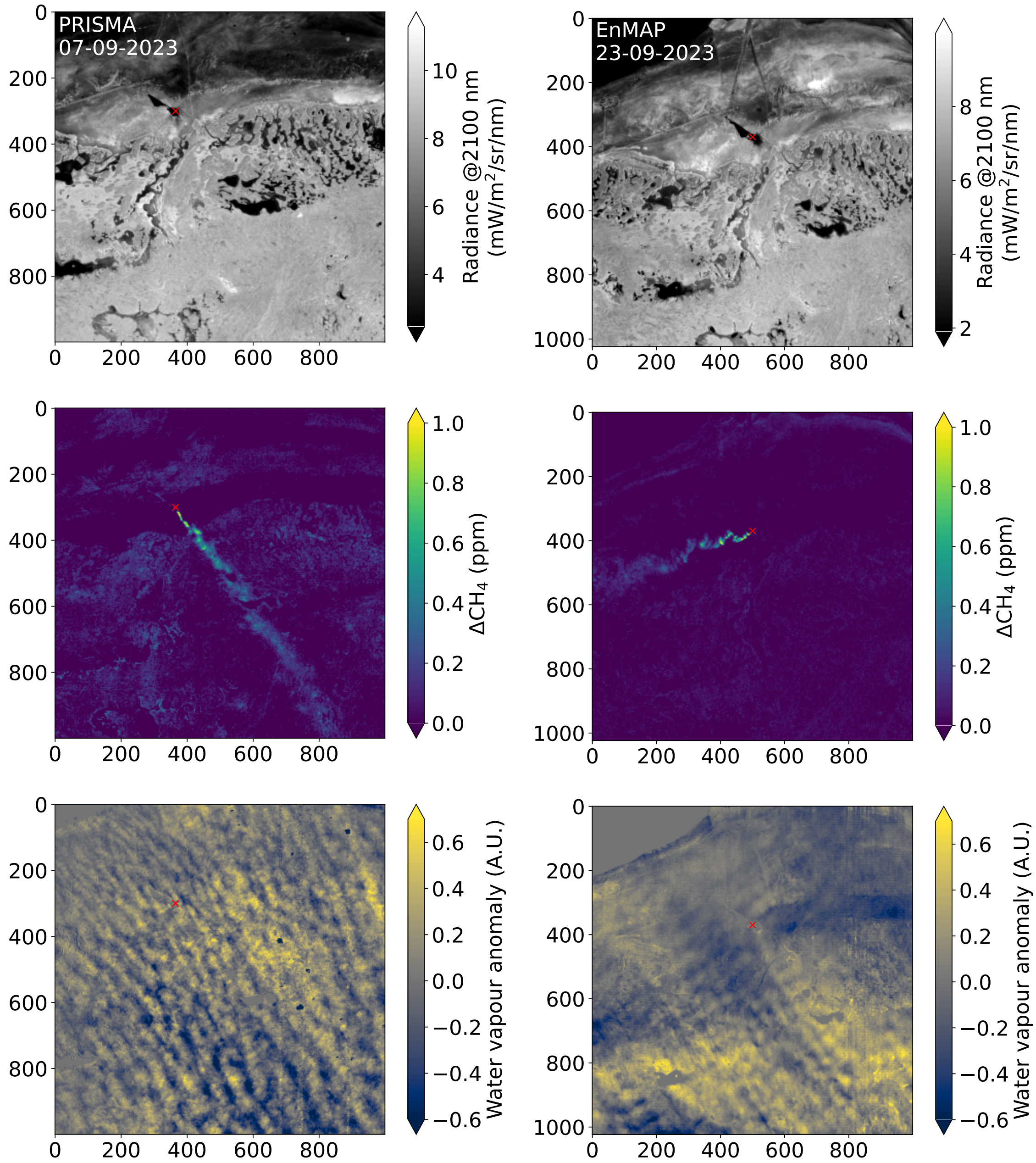

Figure S6: Assessment of the potential distortion of ΔXCH$_4$ retrievals by water vapour and smoke. Maps of at-sensor radiance at 2100 nm (top row), ΔXCH$_4$ (center row), and water vapour concentration anomaly (bottom row) derived from a PRISMA acquisition from 7 September 2023 (left column), and an EnMAP acquisition from 23 September 2023 (right column). No water vapour plume superposed to the methane plume can be observed from the comparison of ΔXCH$_4$ and water vapour anomaly maps. Also, no smoke plume can be observed in the 2100 nm radiance maps, which suggests that, in this particular event, smoke has a negligible optical activity on the shortwave infrared window from which ΔXCH$_4$ maps are retrieved.

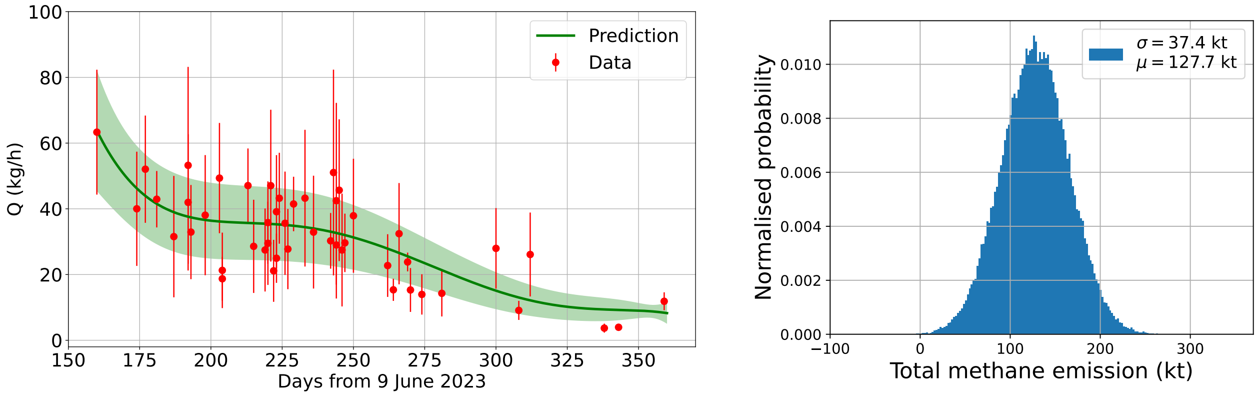

(a) All the high-quality plumes used for the total emission quantification (see Fig. 2a and Fig. S2)

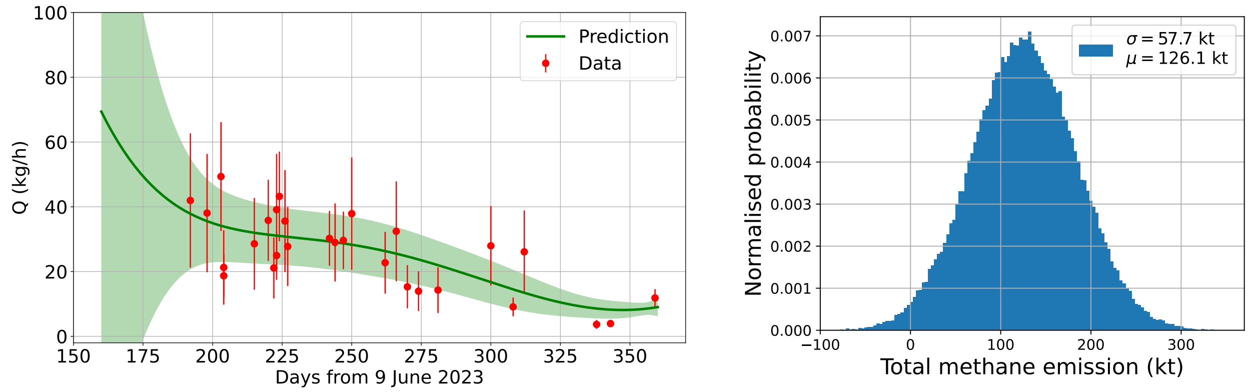

(b) Hyperspectral-only plume detections (PRISMA, EnMAP, EMIT, GHGSat)

Figure S7: Quantification of the total amount of methane released by the leak. The time series on the left hand side depict a polynomial fit of the satellite-based flux rate estimates (Q) selected after quality screening. The fitted model is integrated to obtain an estimate of the total leak. The shaded green area corresponds to the uncertainty (k=1) of the flux rate fitting. The probability distribution functions on the right hand side show the result of propagating the temporal flux rate together with the uncertainty using multivariate Monte Carlo simulations. An error correlation of 0.5 is assumed for the individual satellite observations. The top row shows the results from the dataset consisting of the entire set of satellite observations (TROPOMI as well as hyperspectral and multispectral high-resolution observations) used in this study for the quantification of the leak in this study. The bottom row shows results from the hyperspectral-only case, and illustrates the fact that the extra observations from TROPOMI and the multispectral missions contribute to decrease the uncertainty range but have a very low impact on the total emission estimate.

References

1. Borsdorff, T. *et al.* Measuring carbon monoxide with tropomi: First results and a comparison with ecmwf-ifs analysis data. *Geophysical Research Letters* **45**, 2826–2832 (2018). URL https://agupubs.onlinelibrary.wiley.com/doi/abs/10.1002/2018GL077045. https://agupubs.onlinelibrary.wiley.com/doi/pdf/10.1002/2018GL077045.

2. Powers, J. G. *et al.* The weather research and forecasting model: Overview, system efforts, and future directions. *Bulletin of the American Meteorological Society* **98**, 1717 – 1737 (2017). URL https://journals.ametsoc.org/view/journals/bams/98/8/bams-d-15-00308.1.xml.

3. National Centers for Environmental Prediction, National Weather Service, NOAA, U.S. Department of Commerce. Ncep fnl operational model global tropospheric analyses, continuing from july 1999 (2000). URL https://doi.org/10.5065/D6M043C6.

4. Hersbach, H. *et al.* The era5 global reanalysis. *Quarterly Journal of the Royal Meteorological Society* **146**, 1999–2049 (2020). URL https://rmets.onlinelibrary.wiley.com/doi/abs/10.1002/qj.3803. https://rmets.onlinelibrary.wiley.com/doi/pdf/10.1002/qj.3803.

5. N, K. & P, B. Evaluation of copernicus atmosphere monitoring service methane products (2018).

6. M, C. *et al.* Ghg emissions of all world countries. Scientific analysis or review KJ-NA-30831-EN-N (online),KJ-NA-30831-EN-C (print), Luxembourg (Luxembourg) (2021).

7. Scarpelli, T. R. *et al.* Updated global fuel exploitation inventory (gfei) for methane emissions from the oil, gas, and coal sectors: evaluation with inversions of atmospheric methane observations. *Atmospheric Chemistry and Physics* **22**, 3235–3249 (2022). URL https://acp.copernicus.org/articles/22/3235/2022/.

8. Bloom, A. *et al.* Cms: Global 0.5-deg wetland methane emissions and uncertainty (wetcharts v1.3.1) (2021). URL https://daac.ornl.gov/cgi-bin/dsviewer.pl?ds_id=1915.

9. Jacob, D. J. *et al.* Satellite observations of atmospheric methane and their value for quantifying methane emissions. *Atmospheric Chemistry and Physics* **16**, 14371–14396 (2016). URL https://acp.copernicus.org/articles/16/14371/2016/.

10. Maasakkers, J. D. *et al.* Using satellites to uncover large methane emissions from landfills. *Science Advances* **8**, eabn9683 (2022). URL https://www.science.org/doi/abs/10.1126/sciadv.abn9683. https://www.science.org/doi/pdf/10.1126/sciadv.abn9683.